lubricants

MDPI

Article

Ascorbyl Palmitate-Vitamin C Effective Friction Modifier and Wear Inhibitor for Steel in a PAO Base Oil

Yun Long [1], Jean Michel Martin [1], Frederic Dubreuil [1], Benoit Thiebaut [2], Sophie Loehle [2], Corinne Lacassagne [2] and Maria-Isabel De Barros Bouchet [1,*]

[1] Laboratory of Tribology and System Dynamics CNRS UMR 5513, Ecole Centrale de Lyon, University of Lyon, 36 Avenue Guy de Collongue, 69134 Ecully, France
[2] TotalEnergies OneTech, 69360 Solaize, France
* Correspondence: maria-isabel.de-barros@ec-lyon.fr; Tel.: +33-472186280

Abstract: Ascorbyl palmitate (AP), known as a nutrition pill, and an antioxidant agent in food, has demonstrated excellent lubricity as an additive in PAO4. Adding one wt% AP in PAO4 drastically decreases friction Coefficient (CoF) up to 66% and protects the steel surface from wear. Meanwhile, it shows a more vital friction reduction ability than conventional Mo-based additives and fatty acids, especially palmitic acid. Ascorbic acid core on AP optimises palmitic acid lubricity by forming robust chemical C-O-Fe bond on steel, increasing surface coverage rate. Masked by AP self-assembled layers, steel surfaces can also handle extreme pressure (up to 2.34 GPa) and temperature (150 °C) with unmeasurable wear. This work broadens human-friendly AP vitamin C application for industrial use and introduces a new pathway for optimizing fatty acids lubricity.

Keywords: ascorbyl palmitate; friction modifier; wear inhibitor; self-assembly layer

check for updates

Citation: Long, Y.; Martin, J.M.; Dubreuil, F.; Thiebaut, B.; Loehle, S.; Lacassagne, C.; De Barros Bouchet, M.-I. Ascorbyl Palmitate-Vitamin C Effective Friction Modifier and Wear Inhibitor for Steel in a PAO Base Oil. *Lubricants* **2022**, *10*, 253. https://doi.org/10.3390/lubricants10100253

Received: 11 September 2022
Accepted: 29 September 2022
Published: 11 October 2022

1. Introduction

As a natural component of vegetable oil and animal fats, fatty acids are eco-friendly, disposable, and, most importantly, they are a vital branch of organic friction modifier [1,2] since fatty acids can improve the tribological performance of mineral oil [3] and diesel fuels [4].

Its good lubricity originates from surface separation enabled by alkyl chains as self-assembly fatty acid film possesses a nature thickness. For instance, an alkyl chain with 18 carbon owns a thickness of about 2.2 nm [5]. Meanwhile, alkyl chain length plays a crucial role in tribological performance. Lubricity of fatty acids starts to manifest when the alkyl chain owns more than four carbon atoms and becomes independent of chain length when carbon atoms are above 17 [6]. In between them, lubricity optimises with length increase. To explain how fatty acids lubricate, F. P. Bowden [7] proposed a model where the polar group of fatty acids attaches to substrate surfaces. The alkyl group of fatty acids stretches perpendicularly to substrates; it was later found that fatty acids' stretch direction is on the function of fatty acids' type [8], and the tilt angle is related to the distance between the acid group and its neighbours [9]. Moreover, the linear structure of fatty acid can be modified by unsaturation; this will lead to a deterioration of fatty acid lubricity at boundary lubrication [10] since it impacts the formation of a close-packed layer on substrates [8].

To realise surface separation by fatty acids, the prerequisite condition is the presence of fatty acid molecules in the contact; it has been fulfilled by the chemical adsorption of their acid groups on steel surfaces by forming iron carboxylate [11]. Furthermore, the acid end group shows a stronger adsorption free energy than OH, SH, and Br end-group [12] on ferrous surfaces. Regarding friction reduction, possessing the acid end group is also more efficient than NH_2 and non-polar end groups [13].

Other than fatty acids, fatty acid glycerol ester and fatty amines can also firmly attach to steel surfaces because their carbonyl and hydroxide groups serve as multiple active sites,

leading to salt bridges and hydrogen bond formation between molecules and steel [14]. Molecule attachment can also be achieved by replacing the glycerol end group with the sorbitan function. For example, comparing glycerol monooleate (GMO) and sorbitan monooleate (SMO), SMO owns a superior adsorption rate and a lower friction coefficient (CoF) than GMO in terms of their nanotribological performance [15].

This work proposes a new pathway to facilitate the lubricity of fatty acids and related additives by replacing the carboxylic group of fatty acids with a bigger ascorbic acid core; this vitamin C ester is also called ascorbyl palmitate; its booster effect as an additive in PAO4 has been investigated by performing friction tests under various loads. Afterwards, its lubricity was compared with conventional oil additives and the lubricity mechanism was unveiled byatomic force microscopy (AFM), andX-ray photoelectron spectroscopy (XPS).

2. Materials and Methods

2.1. Materials & Tribometer

Polyalphaolefin 4 (PAO4) was obtained from TotalEnergies (Courbevoie, France). Ascorbyl palmitate-AP (purity $\geq$ 95%), palmitic acid-PA (purity $\geq$ 99%), and stearic acid-SA (purity $\geq$ 95%) were purchased from Sigma-Aldrich (St. Louis, MO, USA). Molybdenum dialkyl dithiocarbamate (MoDTC), Zinc dialkyl dithiophosphate (ZDDP) were received from TotalEnergies. AP molecular structure is in Figure 1a. Solutions of 1 wt% of the additives in PAO4 were prepared by heating their mixtures to 150 °C for 5 min with magnetic stirring. All mixtures are transparent and colourless at 150 °C except the combination of PAO with MoDTC showing a typical yellow-green colour (Figure 1b). AISI 52100 steel balls and disks with a hardness of 8 GPa were bought from PCS Instruments (London, UK). The diameter of the steel balls is 12.7 mm. The roughness of balls and disks are 19.7 nm and 4.4 nm, respectively.

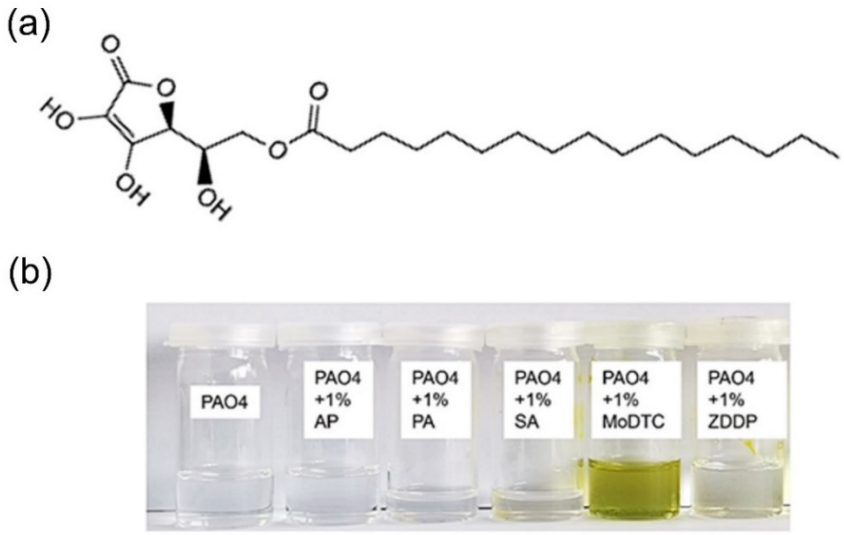

Figure 1. (**a**) Molecular structure of AP. (**b**) Optical pictures of mixtures of PAO4 with one wt% of each additive at 150 °C.

A homemade reciprocating tribometer with a ball-on-flat configuration was used in this study. Details of this tribometer can be found in Guibert's work [16]. A wide range of normal loads from 3 N to 200 N were studied for experimental conditions, corresponding to maximum Hertzian contact pressures (P_{max}) from 0.58 GPa to 2.34 GPa. Sliding speeds from 0.1 mm/s to 10 mm/s were studied, and each test was conducted three times.

2.2. Surface Analysis

After lubricated tests at 150 °C, both steel counterfaces were first rinsed with hot PAO4 (around 150 °C) and then with heptane at ambient temperature to remove AP

and PAO4 residuals. Next, steel surfaces were imaged by digital microscopy (VHX-6000, Keyence, Osaka, Japan), and their roughness and depth profiles were acquired using an interferometer (ContourGT-X, Bruker, Tucson, AZ, USA).

A scanning electron microscope (Microscope SEM MIRA, Tescan GmbH, Gumpoldskirchen, Austria) equipped with an X-ray spectroscopy (EDS) detector was employed to identify topographical and elemental information of wear surfaces.

An atomic force microscope (Park NX10, Park systems, Suwon, South Korea) was used to investigate samples' topographic information and quantify the adhesion force between silicon tips and surfaces by adopting Pinpoint mode.

X-ray photoelectron spectroscopy XPS (ULVAC-PHI Versa Probe II spectrometer where Al Kα (1486.6 eV) serves as X-ray source) was used to analyse steel top surfaces. A take-off angle of 45° was chosen for analysis by adopting corresponding sensitivity factors from [17]. To be sure that probed area does not exceed wear diameter, a 50 × 50 μm^2 area was analysed with a pass energy of 23.5 eV to collect high-resolution O1s spectra.

Wear steel surfaces were also analysed by Raman spectroscopy (Invia^{TM} confocal Raman spectroscopy, Renishaw, Gloucestershire, UK) using a laser of 633 nm wavelength.

3. Results

3.1. Friction and Wear Results

Systematic friction tests have been performed at 150 °C for steel/steel pairs to study the effect of normal force on the tribological behaviour of AP and PAO4. When the steel/steel pair is lubricated by PAO4 alone (Figure 2a) with a normal force of 150 N (P_{max} = 2.12 GPa), the steady-state friction coefficient (CoF) is around 0.15. However, when the normal force is above 150 N, CoF increases to about 0.13. The lowest CoF of 0.125 is obtained when the normal force is 200 N (P_{max} = 2.34 GPa); this trend is completely changed when AP is added to PAO4. When the normal force is below 150 N, the mixture (PAO4 + 1 wt% AP) gives a CoF between 0.05 and 0.06 (Figure 2b). Friction starts to increase when the normal force is above or equal to 150 N. Interestingly, even at 200 N, the steady CoF of steel tribopairs lubricated by PAO4 + AP is still 0.12, less than the case of PAO4 alone.

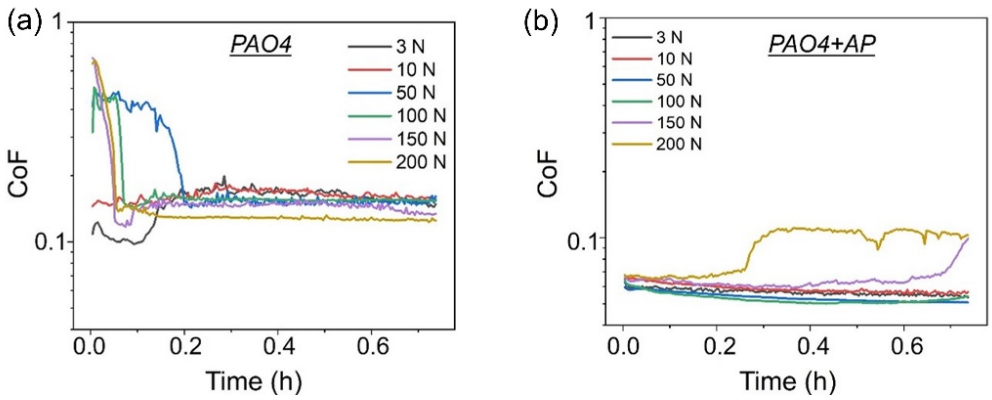

Figure 2. Friction curves under different normal loads at 150 °C lubricated by (**a**) PAO4, (**b**) PAO4 + 1 wt% AP.

Wear has been observed for all steel pairs lubricated by PAO4 alone (Figure 3a). Increasing normal load leads to wear scar diameters larger than Hertzian diameter (Table 1), indicating plastic deformations occur in the wear scar. For example, at 200 N, the wear volume on a steel ball is 3.5 × 10^4 μm^3, and this worn area is partially covered by a blue substance (Figure 3a) while keeping a nearly spherical shape (Figure 3c). The rest of the area is covered by black substances, suffering a strong material missing, and partially loses its spherical shape.

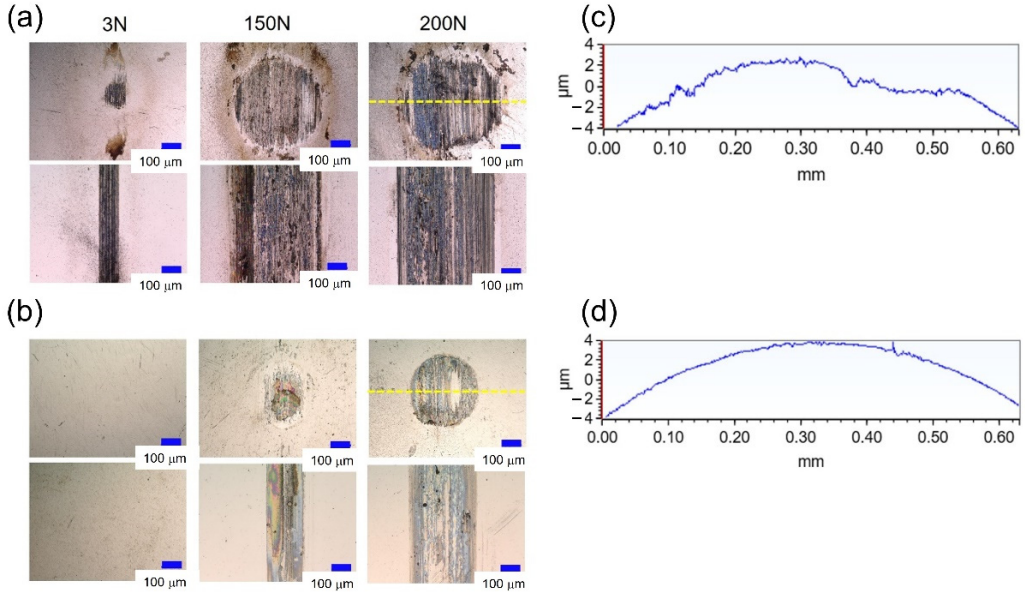

Figure 3. Optical images of wear on balls and flats lubricated by: (**a**) PAO4, (**b**) PAO4 + 1 wt% AP, with ball wear scars images located above disks ones. Here, the scale bar (in blue) is 100 µm. Depth profiles of steel balls at 200 N are lubricated by: (**c**) PAO4, (**d**) PAO4 + 1 wt% AP. Those depth profiles correspond to the yellow line in the left image.

Table 1. Wear diameters of steel balls (D_{ball}) and Hertzian diameter ($D_{Hertzian}$) under different lubrication conditions. P_{max} refers to the maximum Hertzian contact pressure.

Load (N)	3	10	50	100	150	200
P_{max} (GPa)	0.58	0.86	1.47	1.86	2.12	2.34
$D_{Hertzian}$ (µm)	100	174	260	320	360	400
PAO4 + 1 wt% AP						
D_{ball} (µm)	-	-	-	-	195	363
$D_{ball}/D_{Hertzian}$	-	-	-	-	0.54	0.91
PAO4						
Dball (µm)	126	183	400	412	494	516
$D_{ball}/D_{Hertzian}$	1.26	1.05	1.54	1.28	1.37	1.29

On the opposite, when PAO4 + 1 wt% AP mixture is used, wear completely vanishes for all tests performed for normal loads from 3 to 100 N. Steel surfaces are identical to the ones before friction tests. The spherical shape is perfectly conserved without measurable material missing (Figure 3d) and without any coloured areas (Figure 3b); this indicates that only elastic deformation occurred during friction tests.

3.2. Antioxidant Properties of AP under $P_{max} \geq 2.12$ GPa

Coloured substances inside the wear scar (friction test under 150 N load) are studied by SEM/EDS. As shown in Figure 4a, these substances are not homogenously distributed inside the wear track but accumulate at its center. Colourful zones in optical images appear black in SEM imaging, indicating that their material has a lower atomic number than iron. Moreover, layered-like structures are visible inside this zone (Figure 4b), and EDS analysis shows that this zone is masked by a carbon signal (≈85 At%) (Figure 4c). Meanwhile, the iron signal (<5 At%) becomes negligible in carbon-rich zones (Figure 4e). The oxygen content in this carbon-rich zone is around 10 at%, although the oxygen signal covers the whole wear surface of steel (Figure 4d).

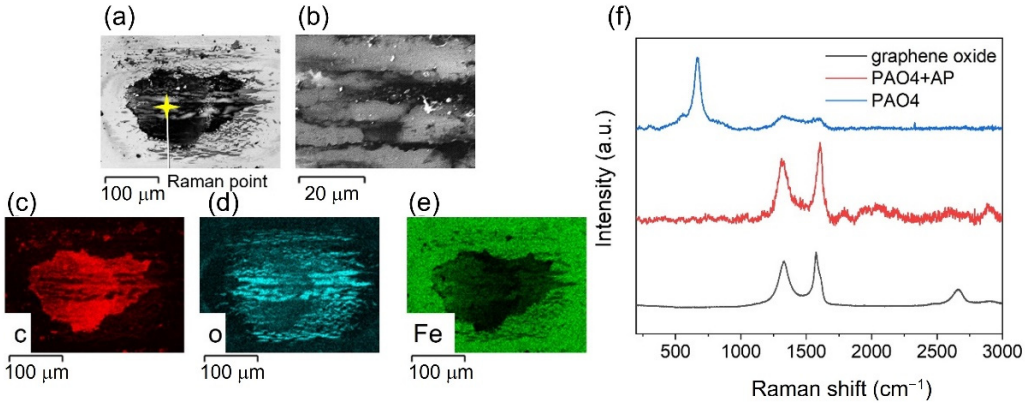

Figure 4. Ball wear scars after lubricated tests by (PAO4 + 1 wt% AP) under 150 N load: (**a**) SEM image (**b**) SEM image of Figure 4a center zone under high magnification. (**c**–**e**) EDS elemental maps of (**c**) carbon, (**d**) oxygen, (**e**) iron. (**f**) Raman spectrum of steel wear lubricated by PAO4 or PAO4 + 1 wt% AP. The spectrum of graphene oxide is also shown for comparison.

Raman analysis of this carbon-rich zone shows D and G peaks of amorphous carbon at 1323 cm^{-1} and 1604 cm^{-1} (Figure 4f). D, G peaks are well known to represent the disordered structure of sp^2 networks of carbon materials. Their locations are different from the D (1330 cm^{-1}) and G (1575 cm^{-1}) peaks of graphene oxide, and no clear 2D peak (2660 cm^{-1}) is present inside wear lubricated by PAO4 + AP; this indicates that this carbon-rich zone does not have the same structure as graphene oxide. It is noteworthy to mention that when steel is lubricated with PAO4 alone, amorphous carbon signals of D (1323 cm^{-1}) and G (1592 cm^{-1}) peaks slightly appear in the wear scar, but a strong magnetite peak [18] at 669 cm^{-1} is also detected.

3.3. Low Friction Properties of AP under $P_{max} \leq 2.12$ GPa

To understand how AP can lubricate steel surfaces when $P_{max} \leq 2.12$ GPa, a 2.5 h-long test has been performed to generate an optically visible wear track, and AFM experiments have been carried out inside the worn area. Results show that measured CoF is below 0.06 (Figure 5a) and a slight colour change from brown to white in wear is observed on the steel disk. Materials removal in wear scar is less than 30 nm in depth.

The steel disk was later analysed by AFM. Scratches are observed on virgin steel surfaces due to polishing (Figure 5f) with a mean roughness Sa of 0.8 nm (scanned area of 2.75 × 2.75 μm^2). The same AFM imaging has also been performed on virgin steel, which was only immersed in PAO4, and similar results were obtained. As expected, PAO4 molecules do not modify the topography of steel. However, after the sliding test in PAO4 + AP, the topography of areas outside wear has changed, and polishing scratches become less visible. Meanwhile, quasi-circular areas with heights around 3 nm lower than other parts are recorded on the steel surface (Figure 6). Those quasi-circular areas have a diameter of around 700 nm (Figure 5d). The topographic change of steel derives from the formation of an inhomogeneous molecular film upon it. Interestingly, the adhesion force in quasi-circular areas is on the same scale (around 25 nN) as in the other parts (Figure 5e), indicating that some molecular film is also presented in quasi-circular areas as the steel surface without molecular film shows an average adhesion force of 65 nN (Figure 5g). As mentioned before, immersing steel in PAO4 does not change its topography. Therefore, this molecular film on the steel surface can only derive from AP. Sa has been altered to 1.2 nm with this inhomogeneous AP film upon steel. Concerning the worn surface, polishing scratches have completely disappeared (Figure 5b), and particles cover the surface with a maximum height of 25 nm regarding the basal plane of steel which doesn't raise the adhesion force between the AFM tip and steel surface. On the contrary, they correspond to the minor adhesion force parts (in the range from 10 to 20 nN) inside wear. The adhesion force in

other areas of steel wear scar is around 33 nN (Figure 5c), significantly smaller than 65 nN, corresponding to the adhesion force between AFM tip and virgin steel (Figure 5g).

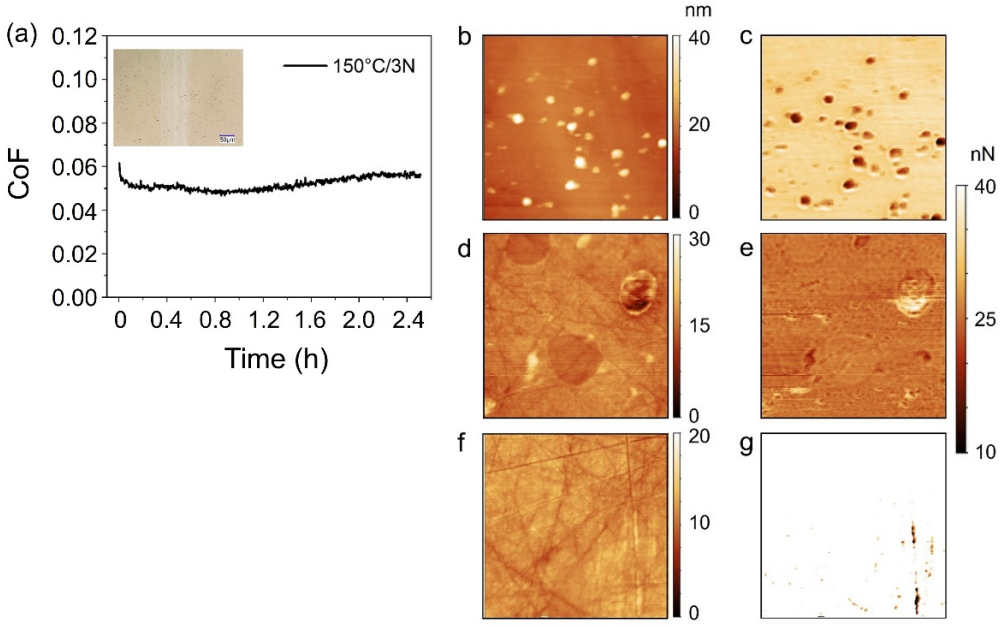

Figure 5. (**a**) friction curve of steel pairs lubricated by PAO4 + 1 wt% AP under 3 N for 2.5 h. The inset image is an optical image of steel wear on the disk. (**b**–**g**) AFM local heights images and adhesion forces images of (**b**,**c**) inside wear, (**d**,**e**)outside wear, (**f**,**g**) virgin steel in an area of 2.75 × 2.75 μm^2. The scale of images (**b**,**e**,**g**) is from 10 to 40 nm. As the majority of virgin steel exceeds this scale range, image g is oversaturated.

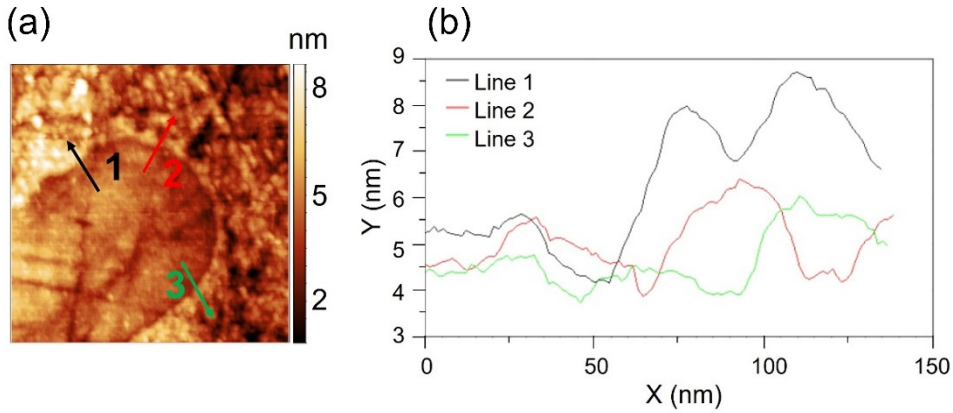

Figure 6. (**a**) AFM local height distribution image of 0.7 × 0.7 μm^2 area, which was performed on part outside disk wear scar after a test of 2.5 h sliding. (**b**) height profiles corresponding to lines 1, 2, and 3 in (**a**).

To conclude, AP can form an inhomogeneous self-assembly film on steel surfaces and reduce adhesion between AFM tip and steel surface. As shearing would cause a redistribution of AP film, a further confirmation of AP presence inside steel wear is still needed despite the low adhesion in the image (Figure 5c) is highly likely associated with AP existence in wear. Therefore, XPS is performed in the following section.

XPS analysis also helps understand how AP interacts with steel surfaces (Figure 7). For all spectra, the O1s FeOx peak locates at around 530.0 eV binding energy (BE) regardless of the calibration methods, in good agreement with the literature [19]. For virgin steel, another critical peak is FeOOH and C-O-Fe peak because both FeOOH [20] and C-O-Fe [21,22] peaks locate at around 531.5 eV. Since the FeOOH/C-O-Fe peak is a mixture of 2 peaks, its

full width at half maximum (FWHM) is 1.6 eV, while FeOx is 1.3 eV (Table 2). Interestingly, the ratio between FeOOH/C-O-Fe peak and FeOx of virgin steel is 0.4 (Figure 7e), but for steel after friction, this ratio is 2.6 regardless of location (Figure 7a,b).

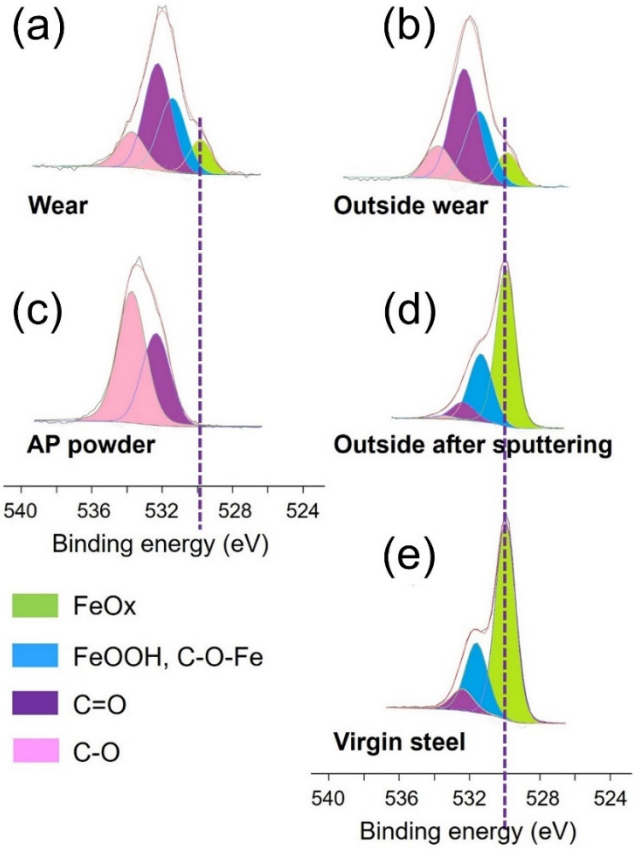

Figure 7. High-resolution O1s peak of (**a**) steel wear after friction test of 2.5 h (**b**) parts outside of steel wear, (**c**) AP powder, (**d**) parts outside steel wear after 15 s sputtering (**e**) virgin steel. Here, (**d**,**e**) are calibrated by indexing the iron oxide peak to 530.0 eV [19]. (**a**–**c**) is calibrated by indexing C1s prominent peak to 284.8 eV.

On the other hand, C-O and C=O peaks located at 532.4 and 533.7 eV BE become more intense after friction on steel flat (Figure 7a,b), where C-O shows a stronger contribution than C=O; this is contrary to the C-O/C=O ratio of AP powder (Figure 7c); this indicates that AP molecules interact with steel and probably iron oxides; this C-O/C=O ratio discrepancy between AP powder and steel flat can be explained by the C-O-H functions of AP converting into C-O-Fe; this also explains why the FeOOH/C-O-Fe peak is more remarkable than FeOx after friction compared with virgin steel. Once steel flat outside wear scar is ion-sputtered for 15 s, carbon content decreases from 61.4% to 5.9% (Table 2). At the same time, FeOx becomes the significant contribution of O1s (Figure 7d), giving evidence that the carbon layer locates on the iron oxide layer; this is consistent with AFM results showing that AP covers steel surfaces.

In summary, AFM and XPS results demonstrate that AP molecules firmly attach to steel surfaces by forming both strong bidentate and monodentate C-O-Fe bonds between AP molecules and the iron oxide layer; this self-assembly molecular layer of AP is robust and survives severe shearing conditions as detected after friction.

Table 2. Elemental contents of different areas were analysed by XPS and XPS fitting details of O1s.

Inside Steel Wear		**O1s**			**C1s**	**Fe2p3/2**
Percentage (%)		**36.6**			**59.2**	**4.2**
	FeOx	**FeOH, C-O-Fe**	**C=O**	**C-O**	**-**	**-**
Position (eV)	529.9	531.4	532.4	533.7	-	-
FHWM (eV)	1.3	1.6	1.6	1.6		
Percentage (%)	3.8	10.9	15.5	6.4		
AP powder	O1s				C1s	Fe2p3/2
Percentage (%)	23.0				77.0	-
	FeOx	FeOH, C-O-Fe	C=O	C-O	-	-
Position (eV)	-	-	532.3	533.7	-	-
FHWM (eV)	-	-	1.9	1.9		
Percentage (%)	-	-	9.7	13.3		
Outside steel wear	O1s				C1s	Fe2p3/2
Percentage (%)	35.4				61.4	3.2
	FeOx	FeOH, C-O-Fe	C=O	C-O	-	-
Position (eV)	529.9	531.4	532.4	533.7	-	-
FHWM (eV)	1.3	1.6	1.6	1.6		
Percentage (%)	3.4	8.9	16.6	6.5		
Outside steel wear after sputtering	O1s				C1s	Fe2p3/2
Percentage (%)	62.1				5.9	32.0
	FeOx	FeOH, C-O-Fe	C=O	C-O	-	-
Position (eV)	530.0	531.4	532.4	533.6	-	-
FHWM (eV)	1.3	1.6	1.6	1.6		
Percentage (%)	37.0	18.7	5.3	1.1		
Virgin steel	O1s				C1s	Fe2p3/2
Percentage (%)	57.2				22.8	20.0
	FeOx	FeOH, C-O-Fe	C=O	C-O	-	-
Position (eV)	530.0	531.5	532.5	-		
FHWM (eV)	1.3	1.6	1.6	-		
Percentage (%)	36.5	14.9	5.8	-		

3.4. Comparison of AP with Conventional Oil Additives

The lubricity of AP as an additive is further compared with well-known conventional oil additives: PA, SA, MoDTC, and ZDDP under 150 °C, 3 N normal load, and sliding speed of 3 mm/s (Figure 8). Adding organic friction modifiers like AP, PA, and SA in PAO4 can efficiently limit the running-in period and initial CoF. At the same time, MoDTC in PAO4 requires ~6 min to decrease the initial CoF from 0.13 to 0.06 (Figure 8a). Regarding ZDDP in PAO4, CoF is always above 0.12. Among those five additives, AP is the most efficient for friction reduction, and it stabilises CoF at around 0.055. Regarding wear, SA, PA (Figure 8c,d) in PAO4 leaves steel disks with minor scratches, with depth below 40 nm, while the scratches of steel wear after lubricated with PAO4 + 1% MoDTC reach 150 nm in depth (Figure 8e). Concerning ZDDP in PAO4, steel wear is covered by colourful tribo-film with a width of 95 µm (Figure 8f). Wear is invisible only when the steel pair is lubricated by PAO4 + 1% AP (Figure 8b). Therefore, compared with conventional oil additives, AP is much more efficient for friction and wear reduction.

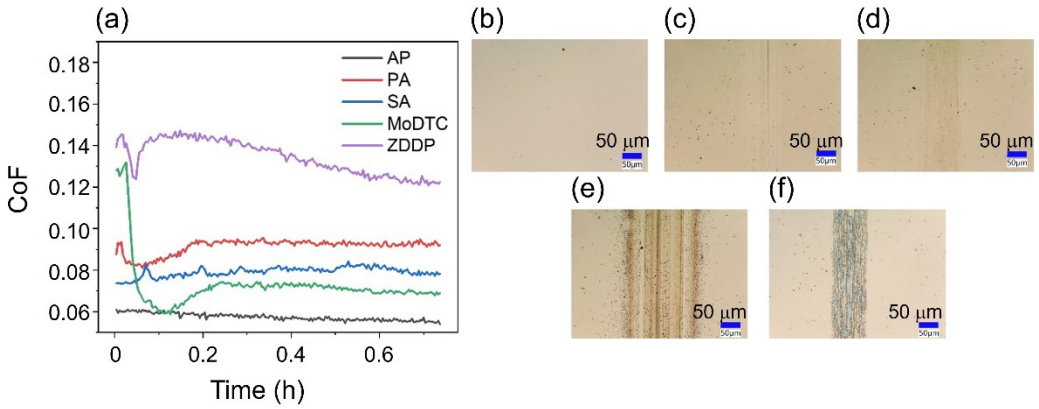

Figure 8. (**a**) Friction curve of steel/steel pair lubricated by PAO + 1% additive at 150 °C, 3 N. (**b**–**f**) optical images of steel wear on disk, which corresponds to steel disk lubricated by: (**b**) PAO4 + 1% AP, (**c**) PAO4 + 1% PA, (**d**) PAO4 + 1% SA, (**e**) PAO4 + 1% MoDTC, (**f**) PAO4 + 1% ZDDP. The scale bar is 50 μm.

4. Discussion

AP is a well-known antioxidant additive in the food industry [23]. Being an ester of ascorbic acid, it is the active component for quenching singlet oxygen [24]; it can also reduce iron from a ferric to a ferrous state and form ferrous ascorbate chelates [25,26]; this could explain why steel pairs lubricated by PAO4 + 1% AP show no iron oxide on steel wear scar by Raman spectroscopy (Figure 4f). Because AP has scavenged active singlet oxygen, steel wear scar shows a stronger C=O signal than C-O one since C-OH of AP becomes C-O-Fe (Figure 7) by forming ferrous ascorbate.

On the other hand, AP shows better friction and wear reduction properties than PA in PAO4 (Figure 8). Simic's group has demonstrated that the steel surface coverage rate of 0.6 wt% palmitic acid PA in PAO 6 is only ~2.7% by AFM [27]. Both friction and wear are strongly associated with PA steel surface coverage rate. However, from our AFM results (Figure 5b–g), the steel coverage rate of AP is practically 100% regardless of the analysed areas. Adding 1 wt% AP in PAO4 increases the surface coverage rate to a value near 100%, driven by the chemical adsorption of AP through bidentate and monodentate bonds on steel surfaces. Due to the robust chemical adsorption and surface protection of AP, wear is beyond measurement when $P_{max} < 2.12$ GPa. Even when $P_{max} \geq 2.12$ GPa, steel surfaces are still protected by AP molecular layers until carbon-based materials accumulate on the steel surface.

Another interesting result is that the lubricity of PAO4 + 1 wt% AP with steel tribopair strongly depends on sliding speed (Figure 9a). Surprisingly, the lowest friction is obtained at 0.1 mm/s at the change of speed direction in the test, and when sliding speed increases from 0.1 mm/s to 5 mm/s, CoF increases to a plateau of 0.06; this CoF-sliding speed correlation has also been found with stearic acid and elaidic acid in hexadecane [28]. In this study, the calculated liquid film thickness using EHL theory [29] at 10 mm/s is about 1 nm, where the viscosity of PAO4 is taken as 3.8 cSt, and the viscosity change due to AP addition is ignored. Because the roughness Sa of steel balls and disks are 19.7 nm and 4.4 nm, the lambda ratio (ratio between liquid film thickness and composite roughness) is well below unity. Therefore, tests are performed from 0.1 to 10 mm/s under severe boundary lubrication conditions.

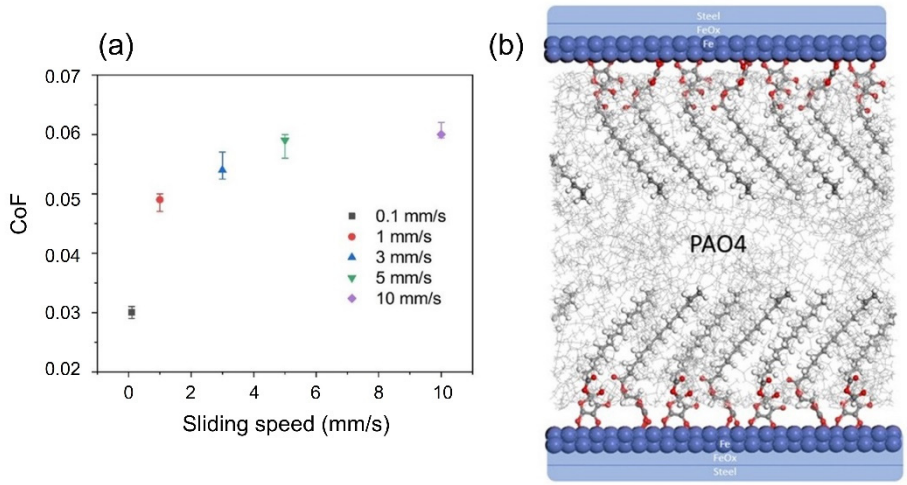

Figure 9. (**a**) friction curve of steel pairs lubricated by PAO4 + 1 wt% AP under different sliding speeds at 150 °C, load 3 N. (**b**) Schematic representation of this low friction system.

Comparing AP with saturated fatty acids, saturated fatty acids avoid steel-steel contact by forming vertically planted close-packed alkyl chains on steel surfaces; this arrangement allows a high surface coverage rate of 4.56 chains per nm^2 [30]. However, in our case, the area of AP's polar head is about 0.46 nm^2 [31] much bigger than for classical saturated fatty acids leading to a steric hindrance increase. Even without considering the intervals among AP molecules, the theoretical maximum surface coverage rate is 2.17 AP chains per nm^2, much less than in the case of classical saturated fatty acids. Thus, the chemisorbed AP layer is less packed than the saturated fatty acid cases, giving a liquid character to the lipophilic part of the monolayer. Due to the relatively large space among AP molecules in the monolayer, PAO molecules may also participate in the formation of the AP monolayer and produce an inter-digital network (Figure 9b). In general, the strong adhesion of AP on iron oxide, its protection against oxidation, and the liquid character of the top of the monolayer could explain the friction/speed correlation and the overall excellent tribological properties of AP as an additive in PAO base oils.

5. Conclusions

This study reveals the excellent lubricity of vitamin C ester-AP as a friction modifier and wear inhibitor in PAO4; its robust friction and wear reduction property survives very high loads till P_{max} of 2.11 GPa. And even when $P_{max} \geq 2.11$ GPa, though its friction reduction property deteriorates, it still protects the steel surface from considerable wear and surface oxidation. The lubricity of AP derives from its unique chemical function. With the ascorbic acid core firmly attaching to the steel surface by forming bidentate C-O-Fe bonds and a surface coverage near 100%, its flexible alkyl chain has a "liquid" character, which favours low energy dissipation when associated with PAO molecules; this finding is undoubtedly helpful in broadening the industrial choice of eco-friendly friction modifiers.

Author Contributions: Conceptualization, M.-I.D.B.B. and J.M.M.; methodology, Y.L. and F.D.; validation, Y.L., formal analysis, Y.L.; writing—original draft preparation, Y.L.; writing—review and editing, all the authors; supervision, M.-I.D.B.B. and J.M.M.; project administration, M.-I.D.B.B.; funding acquisition, S.L., B.T. and C.L. All authors have read and agreed to the published version of the manuscript.

Funding: This research was funded by TotalEnergies OneTech (Solaize Research Center) through a partnership research contact with Laboratory of Tribology and System Dynamics.

Conflicts of Interest: The authors declare no conflict of interest.

References

1. Spikes, H. Friction modifier additives. *Tribol. Lett.* **2015**, *60*, 5. [CrossRef]
2. Kania, D.; Yunus, R.; Omar, R.; Rashid, S.A.; Jan, B.M. A review of biolubricants in drilling fluids: Recent research, performance, and applications. *J. Pet. Sci. Eng.* **2015**, *135*, 177–184. [CrossRef]
3. Syahrullail, S.; Hariz, M.A.M.; Hamid, M.A.; Bakar, A.A. Friction characteristic of mineral oil containing palm fatty acid distillate using four ball tribo-tester. *Procedia Eng.* **2013**, *68*, 166–171. [CrossRef]
4. Bouchet, M.I.D.B.; Martin, J.M.; Forest, C.; Le Mogne, T.; Mazarin, M.; Avila, J.; Asensio, M.C.; Fisher, G.L. Tribochemistry of unsaturated fatty acids as friction modifiers in (bio) diesel fuel. *RSC Adv.* **2017**, *7*, 33120–33131. [CrossRef]
5. Wood, M.H.; Casford, M.T.; Steitz, R.; Zarbakhsh, A.; Welbourn, R.J.L.; Clarke, S.M. Comparative Adsorption of Saturated and Unsaturated Fatty Acids at the Iron Oxide/Oil Interface. *Langmuir* **2016**, *32*, 534–540. [CrossRef]
6. Cottington, R.L.; Shafrin, E.G.; Zisman, W.A. Physical properties of monolayers at the solid/air interface. III. Friction and durability of films on stainless steel. *J. Phys. Chem. C* **1958**, *62*, 513–518. [CrossRef]
7. Bowden, F.P.; Tabor, D. *The Friction and Lubrication of Solids*; Clarendon Press: Oxford, UK, 1971.
8. Abouhadid, F.; Crespo, A.; Morgado, N.; Mazuyer, D.; Cayer-Barrioz, J. Friction Laws for Saturated/Unsaturated Fatty Acid Layers. *Tribol. Lett.* **2021**, *69*, 46. [CrossRef]
9. Ulman, A. Formation and structure of self-assembled monolayers. *Chem. Rev.* **1996**, *96*, 1533–1554. [CrossRef]
10. Doig, M.; Warrens, C.P.; Camp, P.J. Structure and friction of stearic acid and oleic acid films adsorbed on iron oxide surfaces in squalane. *Langmuir* **2014**, *30*, 186–195. [CrossRef]
11. Loehlé, S.; Matta, C.; Minfray, C.; Le Mogne, T.; Iovine, R.; Obara, Y.; Miyamoto, A.; Martin, J.M. Mixed lubrication of steel by C18 fatty acids revisited. Part I: Toward the formation of carboxylate. *Tribol. Int.* **2015**, *82*, 218–227. [CrossRef]
12. Jahanmir, S.; Beltzer, M. Effect of additive molecular structure on friction coefficient and adsorption. *J. Tribol.-T. Asme J.* **1986**, *108*, 109–116. [CrossRef]
13. Fry, B.M.; Chui, M.Y.; Moody, G.; Wong, J.S. Interactions between organic friction modifier additives. *Tribol. Int.* **2020**, *151*, 106438. [CrossRef]
14. Pominov, A.; Müller-Hillebrand, J.; Träg, J.; Zahn, D. Interaction Models and Molecular Simulation Systems of Steel–Organic Friction Modifier Interfaces. *Tribol. Lett.* **2021**, *69*, 14. [CrossRef]
15. Zachariah, Z.; Nalam, P.C.; Ravindra, A.; Raju, A.; Mohanlal, A.; Wang, K.; Castillo, R.V.; Espinosa-Marzal, R.M. Correlation between the adsorption and the nanotribological performance of fatty acid-based organic friction modifiers on stainless steel. *Tribol. Lett.* **2020**, *68*, 11. [CrossRef]
16. Guibert, M.; Nauleau, B.; Kapsa, P.; Rigaud, E. Design and Manufacturing of a Reciprocating Linear Tribometer. In *Journée Francophones de Tribologie: Tribologie et Couplages Multi-Physique, Lille*; Presse Polytechniques et Universitaires Romandes: Lausanne, Switzerland, 2006.
17. Wagner, C.D.; Davis, L.E.; Zeller, M.V.; Taylor, J.A.; Raymond, R.H.; Gale, L.H. Empirical atomic sensitivity factors for quantitative analysis by electron spectroscopy for chemical analysis. *Surf. Interface Anal.* **1981**, *3*, 211–225. [CrossRef]
18. Gunawardana, B.; Swedlund, P.J.; Singhal, N.; Nieuwoudt, M.K. Pentachlorophenol dechlorination with zero valent iron: A Raman and GCMS study of the complex role of surficial iron oxides. *Environ. Sci. Pollut. Res.* **2018**, *25*, 17797–17806. [CrossRef]
19. Biesinger, M.C.; Payne, B.P.; Grosvenor, A.P.; Lau, L.W.; Gerson, A.R.; Smart, R.S.C. Resolving surface chemical states in XPS analysis of first row transition metals, oxides and hydroxides: Cr, Mn, Fe, Co and Ni. *Appl. Surf. Sci.* **2011**, *257*, 2717–2730. [CrossRef]
20. Chagas, P.; Da Silva, A.C.; Passamani, E.C.; Ardisson, J.D.; de Oliveira, L.C.A.; Fabris, J.D.; Paniago, R.M.; Monteiro, D.S.; Pereira, M.C. δ-FeOOH: A superparamagnetic material for controlled heat release under AC magnetic field. *J. Nanopart. Res.* **2013**, *15*, 1544. [CrossRef]
21. Zubir, N.A.; Yacou, C.; Motuzas, J.; Zhang, X.; da Costa, J.C.D. Structural and functional investigation of graphene oxide–Fe_3O_4 nanocomposites for the heterogeneous Fenton-like reaction. *Sci. Rep.* **2014**, *4*, 4594. [CrossRef]
22. Zhou, J.; Song, H.; Ma, L.; Chen, X. Magnetite/graphene nanosheet composites: Interfacial interaction and its impact on the durable high-rate performance in lithium-ion batteries. *RSC Adv.* **2011**, *1*, 782–791. [CrossRef]
23. Kim, T.S.; Decker, E.A.; Lee, J. Antioxidant capacities of α-tocopherol, trolox, ascorbic acid, and ascorbyl palmitate in riboflavin photosensitized oil-in-water emulsions. *Food Chem.* **2012**, *133*, 68–75. [CrossRef]
24. Cort, W.M. Antioxidant activity of tocopherols, ascorbyl palmitate, and ascorbic acid and their mode of action. *JAOCS* **1974**, *51*, 321. [CrossRef] [PubMed]
25. Lynch, S.R.; Cook, J.D. Interaction of vitamin C and iron. *Ann. N. Y. Acad. Sci.* **1980**, *355*, 32–44. [CrossRef] [PubMed]
26. Conrad, M.E.; Schade, S.G. Ascorbic acid chelates in iron absorption: A role for hydrochloric acid and bile. *Gastroenterology* **1968**, *55*, 35–45. [CrossRef]
27. Simič, R.; Kalin, M. Adsorption mechanisms for fatty acids on DLC and steel studied by AFM and tribological experiments. *Appl. Surf. Sci.* **2013**, *283*, 460–470. [CrossRef]
28. Campen, S.; Green, J.H.; Lamb, G.D.; Atkinson, D.; Spikes, H.A. On the increase in boundary friction with sliding speed. *Tribol. Lett.* **2012**, *48*, 237–248. [CrossRef]
29. Nijenbanning, G.; Venner, C.H.; Moes, H. Film Thickness in Elastohydrodynamically Lubricated Elliptic Contacts. *Wear* **1994**, *176*, 217–229. [CrossRef]

30. Ewen, J.P.; Restrepo, S.E.; Morgan, N.; Dini, D. Nonequilibrium molecular dynamics simulations of stearic acid adsorbed on iron surfaces with nanoscale roughness. *Tribol. Int.* **2017**, *107*, 264–273. [CrossRef]
31. Benedini, L.; Schulz, E.P.; Messina, P.V.; Palma, S.D.; Allemandi, D.A.; Schulz, P.C. The ascorbyl palmitate-water system: Phase diagram and state of water. *Colloids Surf. A Physicochem. Eng. Asp.* **2011**, *375*, 178–185. [CrossRef]